Gaia Data Release 3: Ellipsoidal variables with possible black hole or neutron star secondaries

Gomel, R.; Mazeh, T.; Faigler, S.; Bashi, D.; Eyer, Laurent; Rimoldini, Lorenzo; Audard, Marc; Mowlavi, Nami; Holl, Berry; Jevardat De Fombelle, Grégory; Nienartowicz, Krzysztof; Lecoeur-Taibi, Isabelle; Wyrzykowski, L.

A&A 674, A19 (2023)
https://doi.org/10.1051/0004-6361/202243626

Astronomy & Astrophysics
Special issue

Gaia Data Release 3

Gaia Data Release 3

Ellipsoidal variables with possible black hole or neutron star secondaries*

R. Gomel[1], T. Mazeh[1], S. Faigler[1], D. Bashi[1], L. Eyer[2], L. Rimoldini[3], M. Audard[2], N. Mowlavi[2,3], B. Holl[3], G. Jevardat[3], K. Nienartowicz[3], I. Lecoeur[3], and L. Wyrzykowski[4]

[1] School of Physics and Astronomy, Tel Aviv University, Tel Aviv 6997801, Israel
e-mail: roygomel6@gmail.com
[2] Department of Astronomy, University of Geneva, Chemin Pegasi 51, 1290 Versoix, Switzerland
[3] Department of Astronomy, University of Geneva, Chemin d'Ecogia 16, 1290 Versoix, Switzerland
[4] Warsaw University Astronomical Observatory Department of Physics, Al. Ujazdowskie 4, 00-478 Warszawa, Poland

Received 24 March 2022 / Accepted 10 June 2022

ABSTRACT

As part of *Gaia* Data Release 3, a large number of ellipsoidal variables were identified with supervised classification. The periodic variability of these ellipsoidals is presumably induced by tidal interaction with a companion in a close binary system. We present 6306 short-period probable ellipsoidal variables with relatively large-amplitude *Gaia G*-band photometric modulations that indicate a possible massive, undetected secondary. In case of a main-sequence primary, the more massive secondary is probably a compact object – either a black hole or a neutron star, and sometimes a white dwarf. The identification is based on the recently suggested robust modified minimum mass ratio (mMMR) that was derived from the observed ellipsoidal amplitude alone, without the use of the primary mass or radius. We also list a subset of 262 systems with an mMMR higher than unity, for which the probability of a compact secondary is higher. Follow-up observations are needed to verify the true nature of these variables.

Key words. methods: data analysis – techniques: photometric – binaries : close – stars: black holes – stars: neutron – stars: variables: general

1. Introduction

About 20 dynamically confirmed Galactic stellar black holes (BH) are known to reside in close binary systems. All known stellar mass BHs have been discovered through their X-ray emission, which is fuelled by mass transfer from their non-compact stellar companions (e.g., Fabian et al. 1989; Remillard & McClintock 2006; Orosz et al. 2007; Ziolkowski 2014). However, a large fraction of BHs in binaries have probably not been detected so far because their optical counterparts are well within their Roche lobes, so that mass is not transferred and X-rays are not generated, making these systems dormant BHs (see the discussion about the frequency of such systems by Breivik et al. 2017; Mashian & Loeb 2017; Yamaguchi et al. 2018; Shao & Li 2019; Yi et al. 2019; Wiktorowicz et al. 2019; Shikauchi et al. 2020). Similar arguments apply to dormant neutron stars (NSs). Only very few known X-ray binaries harbour an NS companion, while most of similar binaries are probably dormant.

Such a dormant binary can be identified either by a large radial-velocity modulation (e.g., Thompson et al. 2019; Zheng et al. 2019; Clavel et al. 2021; Jayasinghe et al. 2022) or by the large stellar ellipsoidal modulation that is induced by tidal interaction with its compact companion (e.g., Rowan et al. 2021). We aim to identify some of the short-period dormant compact systems through this ellipsoidal effect as revealed by the *Gaia* photometry. A similar study was performed by Gomel et al. (2021c) for the ellipsoidals identified by the OGLE team towards the Galactic bulge (Soszyński et al. 2016).

Based on the observed ellipsoidal amplitude and the estimated mass and radius of the primary star, one can derive a minimum secondary-to-primary mass ratio, defined as the mass ratio obtained for an inclination of 90°, provided most of the light is coming from the primary star (e.g., Faigler & Mazeh 2011; Faigler et al. 2015). A binary with a minimum mass ratio significantly higher than unity might have a dormant compact-object companion, which might be a BH, an NS, or even a white dwarf, depending on the estimated minimum mass of the secondary.

Unfortunately, the primary mass and radius are not well known in many cases. Therefore, Gomel et al. (2021a) presented a simple approach that circumvents this problem by suggesting a robust modified minimum mass ratio (mMMR), assuming the primary fills its Roche lobe. The newly defined mMMR depends on the ellipsoidal amplitude and to some extent (by about a few percent) on the effective temperature of the primary, but it does not depend on the mass or radius of the primary star.

The mMMR is always lower than the minimum mass ratio, which in turn is lower than the actual mass ratio. Therefore, binaries with a high mMMR are likely to host a compact object secondary, even if we cannot reliably constrain their primary mass and radius. This is especially true for binaries with an mMMR higher than unity when the periodic modulation is due to the ellipsoidal effect.

We analyse tens of millions of systems that were classified as possible ellipsoidals with varying degrees of certainty by the *Gaia* DR3 photometric pipeline. We apply our compact companion software to analyse the *Gaia* light curves of these stars to search for systems that might have compact companions.

* Full Table 3 is only available at the CDS via anonymous ftp to cdsarc.cds.unistra.fr (130.79.128.5) or via https://cdsarc.cds.unistra.fr/viz-bin/cat/J/A+A/674/A19

Our analysis is focused on the short-period binaries and tries to avoid systems with primaries that are not on the main sequence (MS). This is because a high mass ratio is not necessarily an indication of a compact companion for giant stars, for example. As discussed by Gomel et al. (2021a), Algol-type binaries, with sub-giant or giant primaries, are famous counterexamples. The mass ratio of these systems, which probably went through a mass-transfer phase during their evolution (e.g., Fedurco & Parimucha 2018; Chen et al. 2020), can be higher than unity and they can still have an MS secondary (e.g., Negu & Tessema 2018; Samadi Ghadim et al. 2018).

In these binaries, a giant, sub-giant, or stripped giant primary is the lower-mass component, but nevertheless is the brighter star of the system (e.g., Nelson & Eggleton 2001; Budding et al. 2004; Mennekens & Vanbeveren 2017). The recently suggested systems consisting of an evolved primary and a dormant compact object secondary (e.g., Thompson et al. 2019; Liu et al. 2019; Rivinius et al. 2020; Jayasinghe et al. 2021) could be Algol-type binaries or even a binary with stripped giant companion (e.g., van den Heuvel & Tauris 2020; Irrgang et al. 2020; Shenar et al. 2020; Bodensteiner et al. 2020; Mazeh & Faigler 2020; El-Badry & Quataert 2021; El-Badry et al. 2022; El-Badry & Burdge 2022). Therefore, a more restricted list of candidates should only include stars that lie on or near the main sequence, with minimum mass ratios higher than unity. This applies to spectroscopic and photometric candidates alike. The analysis resulted in a catalogue of short-period binary candidates that might have compact companions.

Section 2 lists the constraints we used to define our catalogue of 6306 candidate binaries that have mMMRs higher than 0.5 and therefore might have compact object companions, provided their primaries are on the MS and their modulation is induced by the ellipsoidal effect. Section 3 describes the characteristics of the catalogue, Sect. 4 examines the CMD location of a subsample of our candidates, and Sect. 5 cross-matches the catalogue with the available information found in *Gaia* Data Release 2 (DR2), Simbad astronomical database, the International Variable Star Index (VSX) catalogue and in the *Chandra* catalogue of X-ray sources. In Sect. 6, we narrow the catalogue and identify 262 binaries with an mMMR significantly higher than unity, and we present their folded light curves and fitted ellipsoidal modulations. Section 7 presents some details of three stars from the catalogue as examples by comparing the *Gaia* light curves with OGLE, ASAS-SN, and ZTF photometry. We plot these stars in red in the diagrams of the paper. Finally, Sect. 8 discusses and summarises our findings.

2. Defining the catalogue

The compact companion software, which is part of the variability analysis software (VariPipe, Eyer et al. 2023), identified ~20 million possible ellipsoidal systems, obtained by combining multiple classifiers (Rimoldini et al. 2023), with different ellipsoidal probability selection cuts. We searched this large sample for ellipsoidals with possible compact object companions.

In our analysis we used mainly the G light curve (Rimoldini et al. 2022), as only a small fraction of systems had enough $G_{\rm BP}$ or $G_{\rm RP}$ measurements to derive significant amplitudes. For these, we were unable to detect any colour-based clustering, and therefore we used the colour information only to remove three outlier systems.

We used the cleaned G light curve, folded with P, twice the period found by a generalised Lomb-Scargle (GLS) period search (Zechmeister & Kürster 2009), as we assumed that the *Gaia* pipeline detected the predominant second-harmonic periodicity of the ellipsoidal. The period uncertainty, $P_{\rm err}$, was derived by the pipeline.

We included only systems with more than 25 cleaned G field-of-view (FoV) transits, with a period within $0.25 < P < 2.5$ d, $P/P_{\rm err} > 10$, and with a frequencygram peak[1] >12 to ensure that the adopted period was genuine and significant. The upper limit of the second condition was used to avoid systems with non-MS primaries.

As shown by Gomel et al. (2021c), the period of ellipsoidal variables with MS primaries in most cases is shorter than 2.5 days. At this stage, we were left with 112 591 candidates.

Next, a three-harmonic model was fitted to each light curve,

$$G_{\rm mag} = \overline{G} + \sum_{i=1}^{3} a_{ic}\cos\left(\frac{2\pi i}{P}(t-T_0)\right) + a_{is}\sin\left(\frac{2\pi i}{P}(t-T_0)\right), \quad (1)$$

with seven free parameters, $\overline{G}, a_{ic}, a_{is}$, $\{i = 1,2,3\}$, that characterise the presumed periodic modulation. Each parameter was derived with its corresponding uncertainty. T_0 was chosen so that $a_{2s} = 0$. We defined the amplitude of each harmonic as

$$A_i = \sqrt{a_{ic}^2 + a_{is}^2} \ \{i = 1,2,3\}. \quad (2)$$

In the next stage of searching for candidates with compact object companions, we chose only systems with $0.33 < A_2/(\text{range of } G) < 0.6$, $A_2/A_{2,\rm err} > 10$, $A_1/A_{1,\rm err} > 3$ or $A_3/A_{3,\rm err} > 3$, and $A_1/A_2 < 1$ together with $A_3/A_2 < 0.3$.

The first two conditions were set to obtain a reliable and significant A_2. Third condition reflected our expectation for an ellipsoidal light curve to display non-equal minima, and the harmonic ratio of the fourth condition is typical for ellipsoidals. We were left with a sample of 22 914 systems that are highly probable short-period ellipsoidal variables.

The $\overline{G}$-mag histogram of the 22 914 systems is shown in Fig. 1. This magnitude was derived with Eq. (1) and is slightly different from a simple arithmetic mean. It is evident that most systems are relatively faint, covering a $\overline{G}$-mag range of 13–20. In the figure we added the 19th mag mark to denote the observational limit of a few existing multi-object spectrographs that can be used to follow the best candidates (see discussion in Sect. 8).

The final stage of constructing the catalogue of candidates was to identify ellipsoidals that might have compact companions. This was done using Eq. (1) of Gomel et al. (2021a), which estimates the leading amplitude A_2 of the ellipsoidal as a function of the fillout factor f. This equation combines the primary volume-averaged radius divided by its Roche-lobe volume-averaged radius (Kopal 1959; Paczyński 1971), the orbital inclination i, and the secondary-to-primary mass ratio q,

$$A_2 \simeq \frac{1}{\overline{L}/L_0}\alpha_2\, f^3 E^3(q)\, q\, \sin^2 i\, C(q,f), \quad (3)$$

where $\overline{L}$ is the average luminosity of the star, L_0 is the stellar brightness without any secondary, and $E(q)$ is the Eggleton (1983) approximation for the volume-averaged Roche-lobe radius in binary semi-major axis units. The ellipsoidal coefficient α_2 depends on the linear limb- and gravity-darkening coefficients of the primary and is expected to be in the 1–2 range. The correction coefficient $C(q,f)$ starts at 1 for $f = 0$ (no correction), as

[1] Measures the height of the frequencygram peak relative to the frequencygram mean in units of the standard deviation of the frequencygram.

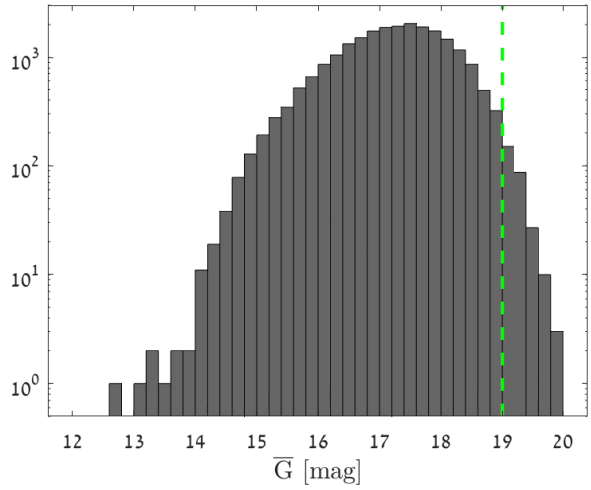

Fig. 1. Histogram of $\overline{G}$ of 22 914 compact companion candidates. The 19th mag vertical dashed green line marks the observational limit of a few existing multi-object spectrographs that can be used to follow the candidates (see the discussion in Sect. 8).

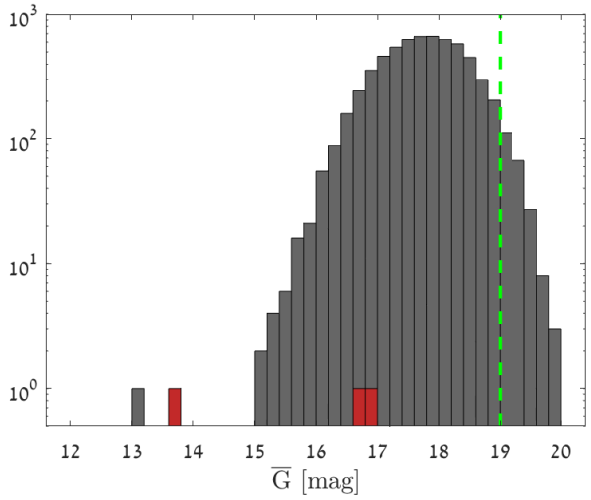

Fig. 2. Histogram of $\overline{G}$ of 6306 compact companion candidates. The three sources discussed in Sect. 7 are shown in red. For the green line, see Fig. 1.

expected, and rises monotonically as $f \rightarrow 1$, obtaining a value of ∼1.5 at $f \gtrsim 0.9$ (Gomel et al. 2021b).

Assuming a fillout factor of $f = 0.95$, an inclination of 90°, and a typical α_2 of 1.3 for the G band (Claret 2019), we solved for the mMMR, $\hat{q}_{\rm min}$, (Gomel et al. 2021a), based on the observed second harmonic amplitude A_2. We set f to be 0.95 to be able to use the analytical approximation of Gomel et al. (2021b). The mMMR value obtained for a fillout factor of unity would be lower than the value we derived.

The uncertainty of $\hat{q}_{\rm min}$ is inherently high because A_2 increases asymptotically as a function of q and because of the uncertainty in the ellipsoidal amplitude approximation we use. In particular, α_2 is not well known, therefore we adopted its uncertainty to be 0.1. We then derived the uncertainty of A_2/α_2, and assuming a Gaussian distribution for this ratio, using Eq. (3), we obtained $\hat{q}_{\rm min}^{-1\sigma}$, which corresponds to the 15.9 percentile of A_2/α_2. In a similar way, we derived $\hat{q}_{\rm min}^{-3\sigma}$, which corresponds to the 0.135 percentile of A_2/α_2.

As pointed out by Gomel et al. (2021a), the mMMR is expected to be lower than the actual mass ratio of the system because it assumes a fillout factor close to unity and an inclination of 90°. Therefore, we somewhat arbitrarily opted to include systems with $\hat{q}_{\rm min} > 0.5$ in our catalogue of ellipsoidals that might have compact companions. This resulted in 6336 candidates. Different thresholds would have yielded different catalogues. In particular, adopting a different fillout factor, for instance, of $f = 0.98$ to solve Eq. (3) would yield a smaller catalogue.

The adopted catalogue included 27 sources that were identified as RR Lyrae variables, 25 of which are known RR Lyrae stars in the Milky Way bulge, 24 sources from the OGLE survey (Soszyński et al. 2014) and one source from the VVV survey (Contreras Ramos et al. 2018). Two additional sources are not known in the literature but were confirmed as RR Lyrae stars by inspecting their light curves. Therefore we exlcuded the 27 presumably RR Lyrae variables from the final list.

Analysis of the $G_{\rm RP}$ and $G_{\rm BP}$ light curves yielded only a small number of systems with periodic colour information significant enough for our use. We derived the second-harmonic amplitude $A_{2,\rm RP}$ by using equation (1) for the $G_{\rm RP}$ light curve and inspected the $A_{2,\rm RP}/A_2$ distribution for the 815 systems with $A_{2,\rm RP}/A_{2,\rm RP,err} > 10$. We found three outliers with amplitude ratios lower than 0.7 that we excluded from the catalogue. This left 6306 candidate ellipsoidal variables with compact companion secondaries.

The resulting catalogue of 6306 short-period ellipsoidals is given online in the DR3 archival data in table `gaia_dr3.vari_compact_companion`. The first 15 candidate are described in detail in Sect. 6.

3. Catalogue

This section presents some characteristics of the catalogue of the compact companion candidates. Figure 2 shows the $\overline{G}$-mag histogram of the candidates as derived by Eq. (1). The figure shows that most of the compact companion candidates are relatively faint, in a $\overline{G}$-mag range of 15–20. Two brighter sources lie within 13–14 mag, and one of these sources is discussed in Sect. 7.

A density distribution of the 6306 catalogue stars in Galactic coordinates, coloured according to the orbital period, is presented in Fig. 3. The candidates are spread thorughout the Galactic disk, and most of them are located towards the bulge. Interestingly, the 59 known X-ray binaries (e.g., Corral-Santana et al. 2016) are also concentrated in the Galactic disk, as shown in the figure.

Our ability to identify ellipsoidals, and compact object candidates in particular, clearly depends on the number of FoV transits. This is reflected in Fig. 4, which displays the distribution of the number of G-band FoV transits for the 6306 candidates. Our imposed lower limit of $N = 25$ is evident. The number of G-band FoV transits varies between 25 and 130, with a median value of 46.

The amplitude of the second harmonic A_2 and the mMMR, $\hat{q}_{\rm min}$, are plotted in Fig. 5 as a function of the orbital period P. Each value of A_2 corresponds to a unique value of $\hat{q}_{\rm min}$ as obtained from Eq. (3). The distributions of A_2, $\hat{q}_{\rm min}$ and P are plotted alongside their axes.

As mentioned above, we focused on short-period systems with orbital periods between 0.25–2.5 d, while the lower limit of $A_2 \sim 0.66$ mag corresponds to a minimum value of $\hat{q}_{\rm min} = 0.5$,

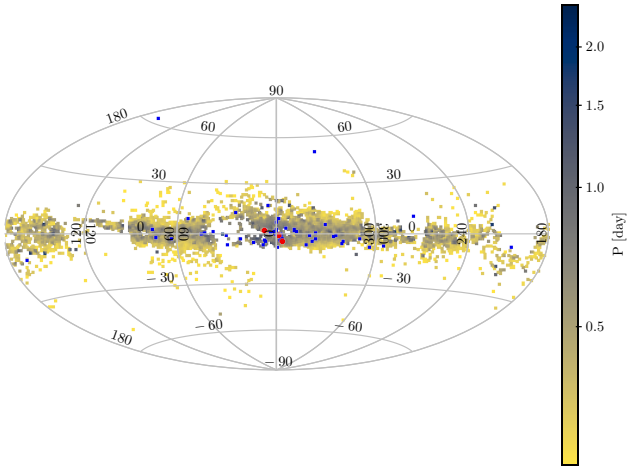

Fig. 3. Density distribution of the 6306 compact companion candidates in Galactic coordinates, coloured according to orbital period. The three sources discussed in Sect. 7 are shown in red. The 59 Galactic X-ray binaries are shown by blue points. The conspicuous circular hole between Galactic longitudes of ∼10 and ∼40 deg is due to the *Gaia* scan law and our imposed lower limit of 25 FoV transits.

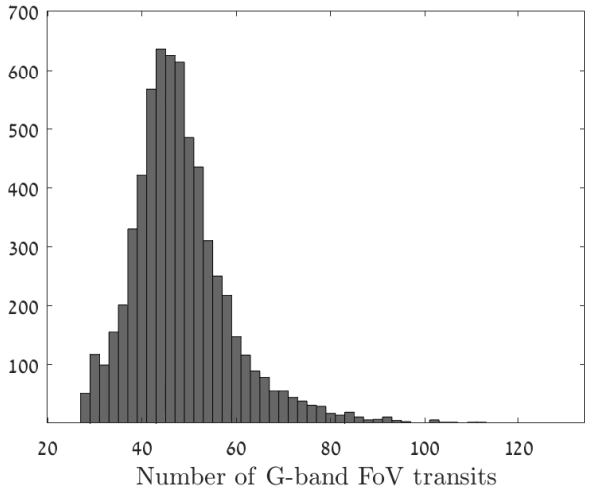

Fig. 4. Histogram of the number of G-band FoV transits for 6306 compact companion candidates. The lower limit of $N = 25$ was imposed by our analysis.

which defines our catalogue of compact companion candidates. Since we chose our catalogue to include only systems with relatively large A_2 and a significant frequencygram peak, we expect a minor contamination, if any, of spurious periods caused by the *Gaia* scanning law. A slight deficit of low-amplitude systems might be noted in Fig. 5 around $P \sim 0.5$ d. This could be a result of our pipeline (Sect. 2), which was sensitive to the *Gaia* 6-h orbital spin.

4. Location of the candidates in the CMD

As mentioned above, we are interested in ellipsoidal variables with primaries that are not giants or sub-giants. To determine whether this is indeed the case, we plot in Fig. 6 the position of a sub-sample of our candidates in the *Gaia* colour–magnitude-diagram (CMD). Only 513 candidates were included. The relative parallax precision for them was better than 20% ($\varpi/\sigma_\varpi >$ 5), the parallax was higher than 0.5 mas ($\varpi >$ 0.5 mas), and a *Gaia* extinction estimate was available.

The location of the sub-sample in the CMD is shown after correcting for their extinction, taken from *Gaia* DR3 data (Fouesneau et al. 2023). As a background we plot the *Gaia* stars that have the same characteristics as the ellipsoidal sub-sample, but have a relative parallax precision better than 10%. The background stars mark the location of the MS, and even the red clump is visible in the upper part of the figure. We also added two theoretical (green) curves that mark the expected edges of the MS, as derived with the ISOCHRONE[2] software package (Morton 2015).

Figure 6 clearly shows that at least for the plotted sub-sample, we succeeded to avoid the giant and the sub-giant branch of the CMD, probably due to the period limit of 2.5 days. Therefore, if the candidates are indeed ellipsoidals and if their mass ratios are higher than unity, they might have compact companions.

We note, however, that the minimum mass ratio of our sample is 0.5 because we chose candidates with $\hat{q}_{\rm min} > 0.5$, and therefore the secondary of many of our candidates can still be a MS component. This is probably reflected in the figure, which shows the location of quite a few of the candidates above the MS, possibly due to the light contribution of the MS secondary. To show this point, we plot in the figure (dashed blue curve) the theoretical upper G value that is expected for binaries with two MS stars, which was obtained by shifting the upper bound of the MS by 0.75 mag.

However, we emphasise that CMD locations can contain large uncertainties in absolute G due to errors in parallax, photometry, and extinction estimates, which may be highly inaccurate (Gaia Collaboration 2018; Andrae et al. 2018; Anders et al. 2019). In addition, the extinction uncertainty can shift the $G_{\rm BP} - G_{\rm RP}$ colour index. We demonstrate this point by plotting nine candidates for which the minimum mass ratio is higher than unity, as discussed in Sect. 6. Their companions are less likely to be on the MS, but the locations of six of them nevertheless appear above the MS. For these, we plot the G 1σ uncertainty, showing that all six systems might still be, within 1 or 2σ, on the MS strip.

We note that the figure suggests that many of the candidates in our sample might have a mass lower than 0.8 $M_\odot$, for example. Consequently, their compact companions might have a relatively low mass in the white dwarf range.

5. Cross-match with *Gaia* DR2, Simbad, *Chandra*, and VSX

In this section we cross-match our catalogue with the Simbad astronomical database[6], with the *Gaia* DR2 variability data set (Gaia Collaboration 2018), with the *Chandra* source catalogue[7] release 2.0, and with the VSX catalogue[8].

5.1. Cross-match with the Simbad catalogue

The cross-match with Simbad used a search radius of 3″ and resulted in 528 systems. They are summarised in Table 1. The cross-match yielded 522 stars classified as variables and 6 additional systems without a main identifier of variability. Two

[2] https://github.com/timothydmorton/isochrones
[6] https://simbad.u-strasbg.fr/simbad/
[7] https://cxc.cfa.harvard.edu/csc/
[8] https://www.aavso.org/vsx/

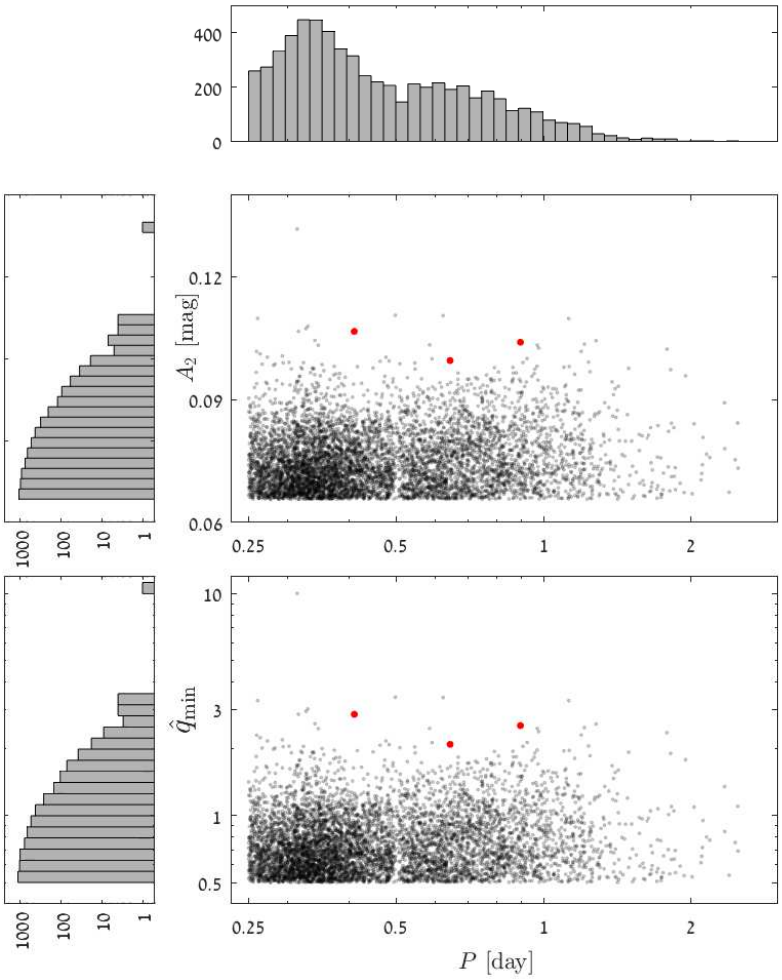

Fig. 5. Second-harmonic amplitude (A_2) and mMMR ($\hat{q}_{\rm min}$) as a function of orbital period (P) for the 6306 compact companion candidates. The mMMR was derived using a typical α_2 of 1.3 for the G band and assuming a fillout factor of 0.95. The three sources discussed in Sect. 7 are shown in red.

out of the 6 systems were detected by the *Chandra* mission (Evans et al. 2010) as having significant X-ray emission.

Most systems that our catalogue has in common with the Simbad catalogue were classified by the OGLE team as eclipsing binaries. We inspected a few dozen of them and found in all cases that the OGLE I and *Gaia* G light curves did not present clear narrow or flat-bottom eclipses. They showed possible very broad two V-shape eclipses, if any, centred around phases 0 and 0.5, suggesting they might either be contact binaries or ellipsoidal variables. It is difficult to differentiate between the two modulations because they are both spread over the entire binary-period phase and have similar shapes. Nevertheless, we suggest that the contamination of the catalogue by contact binaries is small, as discussed in Sect. 8.

We visually inspected the modulation of the two stars identified by OGLE as RR Lyrae variables (*Gaia* DR3 4116610292178919936, 4107297257038868736) and found that the OGLE classification is more probable, at least for the second object. The fact that only two cases were found as RR Lyrae stars out of 528 cross-matched systems suggests that about half a percent of the stars of our catalogue might be RR Lyrae variables.

5.2. Cross-match with Gaia DR2 variables

A cross-match of the candidate list with the *Gaia* DR2 variability data set (Gaia Collaboration 2018), resulted in two systems, 2024410711652386560 and 241721038597143296. The two sources were classified as rotational variables, with a rotational period that is half the value presented in our catalogue. Our analysis suggests that they are really ellipsoidal variables, however. None of the sources appears in the Simbad database.

5.3. Cross-match with the Chandra source catalogue

A cross-match of the candidate list with the *Chandra* source catalogue (Evans et al. 2010), using a search radius of 1″, resulted in three systems that are presented in Table 2. They are all included in Table 1. The third object, *Gaia* DR3 5966509571940818048, is in the category "Other stars", classified by Simbad as a candidate young stellar object. Its X-ray flux is $\sim 2 \times 10^{-15}$ erg cm^{-2} s^{-1}, with a relatively soft spectrum, consistent with the X-ray luminosity (derived from its *Gaia* EDR3 parallax) coming from the stellar surface. The other two X-ray sources are too faint for a significant flux measurement.

5.4. Cross-match with the VSX catalogue

Following the referee's suggestion, we cross-matched our candidates with the VSX catalogue[9] and found 2044 common systems with derived periodicities and available light curves. Figure 7 shows the VSX periods versus those from *Gaia*. Most systems (1853) have identical periods in the two catalogues. Some systems (175) display a VSX period that is half the *Gaia* period,

[9] https://www.aavso.org/vsx/

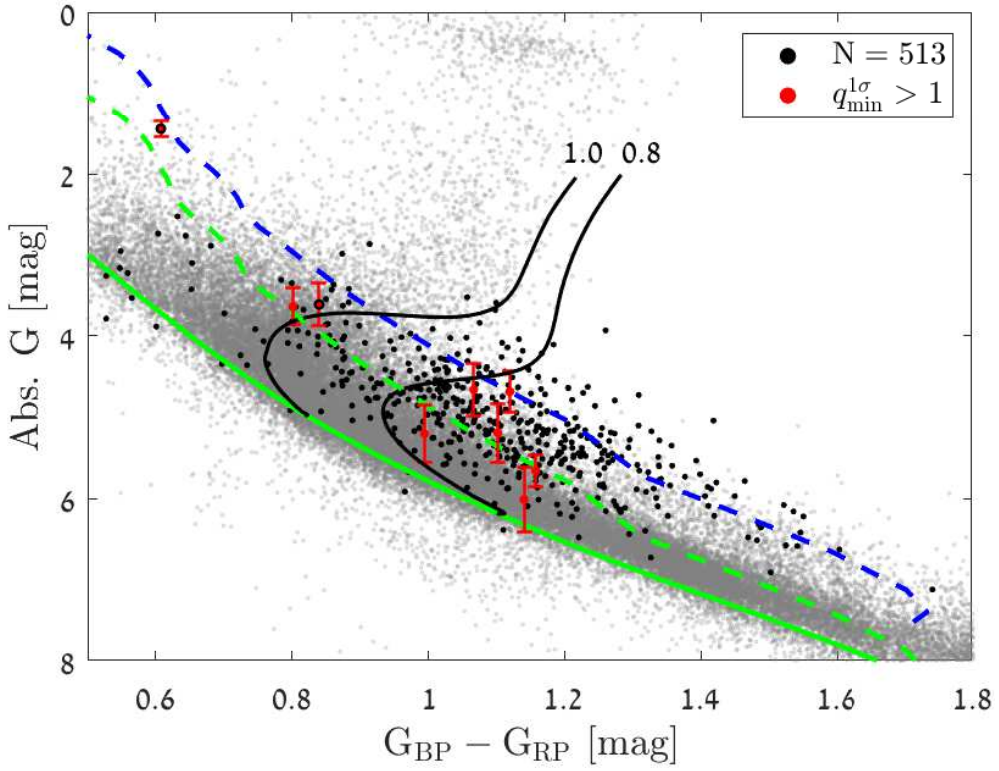

Fig. 6. Compact companion candidates in the extinction-corrected *Gaia* CMD. Only 513 candidates with a minimum parallax of 0.5 mas and parallax-over-error > 5 are plotted. The background grey-scale density map of stars with a minimum parallax of 0.5 mas and a parallax-over-error > 10 serves as a proxy for the expected CMD. Magnitudes and extinction corrections for the candidates and the background stars are from *Gaia* DR3 data (Fouesneau et al. 2023). Nine systems with $\hat{q}_{\min} > 1$ are plotted in red (see text). The two green curves mark the theoretical expected edges of the MS. The dashed blue curve is the theoretical upper G value expected for binaries with two identical MS stars, obtained by shifting the upper bound of the MS by 0.75 mag. We show the evolutionary tracks of 0.8 and 1 $M_{\odot}$ stars within their MS phase in black. They were obtained with the ISOCHRONE[5] software. The two sources DR3 4042390512917208960 (upper point) and DR3 4056017172771375616 (lower point) are discussed in Sect. 7 and are shown in red with a black edge.

Table 1. Cross-match classifications of 528 candidates obtained from the Simbad database.

Classification	Number	Source
Eclipsing binaries	431	OGLE survey
	9	CRTS survey (Drake et al. 2014)
	7	BEST II catalogue of variable stars (Fruth et al. 2013)
	2	Miller et al. (2010)
	1	General catalogue of variable stars (Samus' et al. 2017)
	1	de Marchi et al. (2010)
	1	Weldrake & Bayliss (2008)
Ellipsoidal variables	65	OGLE survey
RR Lyrae stars	2	OGLE survey
Rotational variable	1	CRTS survey (Drake et al. 2014)
Delta Scuti	1	BEST II catalogue of variable stars (Fruth et al. 2013)
Orion-type variable	1	Rebull (2001)
X-ray sources	2	Muno et al. (2003, 2006)
Other stars	4	Metzger & Schechter (1998), Bernabei & Polcaro (2001); Audard et al. (2007), Kuhn et al. (2017)

consistent with them being ellipsoidal variables for which the dominant frequency of the modulation is the second harmonic.

Three sources (shown as blue circles in Fig. 7), *Gaia* DR3 4615213114306434 56, *Gaia* DR3 1834964858132757504, and *Gaia* DR3 1825053924741093376, analysed by the ZTF project (Bellm et al. 2019), display a clear discrepancy between the *Gaia* and the VSX periods. We re-analysed the ZTF light curves of the three systems[10] by deriving their corresponding power spectra, as shown in Fig. 8. The frequencies of the strongest

[10] https://irsa.ipac.caltech.edu/Missions/ztf.html

Table 2. Cross-match with the *Chandra* source catalogue.

Gaia DR3	Name
4056853999874300544	2CXO J174344.8−295445
4057484501078108800	2CXO J174512.0−285756
5966509571940818048	2CXO J165419.4−414805

peaks of the three ZTF power spectra are within 1σ of the corresponding *Gaia* frequencies.

The spectra are dominated by strong side lobes on the two sides of the strongest peak, separated by $\Delta f = 1$, reflecting the daily window of ground-based observations. The frequencies of the highest peaks of the three systems, which correspond to half the *Gaia* orbital periods, are close to a whole number, in units of 1/day, and therefore have one side-lobe peak with a low frequency, as shown in the figure. This side lobe corresponds to the period suggested by the ZTF analysis. This exercise shows the potential advantage of space-mission measurements, which are not subject to the daily cycle of ground-based observations.

6. Candidates with an mMMR higher than unity

We chose 262 ellipsoidals with $\hat{q}_{\rm min}^{-1\sigma} > 1$, which we considered to have an mMMR significantly higher than unity. This makes them more promising candidates for having compact companions. Forty one of these candidates were found in Simbad, 39 of which are classified as eclipsing binaries and 2 as ellipsoidals by the OGLE project (Soszyński et al. 2016). One of the two ellipsoidals is relatively bright, with a G magnitude of ∼13.8, and is discussed in detail in Sect. 7.

Folded light curves and a summary table for the first 15 candidates, in descending $\hat{q}_{\rm min}$ order, are presented in Fig. 9 and Table 3. Similar figures and a table for all 262 candidates are given in the online supplementary document[11]. The full Table 3 is also available at the CDS. The table includes the *Gaia* DR3 identifier (id), *Gaia* orbital period, reference time T_0 [BJD-2455197.5], which was chosen so that $a_{2s} = 0$, average G magnitude $\overline{G}$, and the cosine and sine Fourier coefficients $a_{ic}, a_{is}\,\{i = 1, 2, 3\}$ of the three-harmonic model, defined by Eq. (1), each with its uncertainty. The table also gives the total number of G-band FoV transits, N, the derived mMMR, and the lower-percentile mMMR.

All included parameters of Table 3, except for N, are given online in the DR3 archival data, in the table `gaia_dr3.vari_compact_companion`. The archival data also include reference times, averaged magnitudes, and Fourier coefficients with their uncertainties for the *Gaia* $G_{\rm BP}$ and $G_{\rm RP}$ light curves, the 0.135th percentile mMMR, $\hat{q}_{\rm min}^{-3\sigma}$, and the ellipsoidal coefficient α_2, defined in Eq. (3).

Out of the 262 light curves, the light curve of *Gaia* DR3 4068402346632484864 has an untypical shape for ellipsoidal variables, as shown in Fig. 9 (marked in bold), suggesting that this star is an RR Lyrae variable. This is consistent with the above discussion that our catalogue is contaminated by ∼1% of RR Lyrae stars.

A close look at Fig. 9 might give the impression that the two maxima of some of the light curves have different heights. This is reflected by the difference between the coefficient of a_{1s} and a_{3s}, indicating either that the light curves are not due to an ellipsoidal modulation or that we are witnessing an additional effect. However, this is probably not the case. The *Gaia* data are quite sparse and in many cases not sufficient to identify such local small features of the modulation. One good example is *Gaia* DR3 4056017172771375616, discussed in the next section, in which the *Gaia* model, based on only 44 measurements, does display two different peaks, while the OGLE light curve, with 70 points, shows equal maxima.

[11] https://zenodo.org/record/6686715#.YrNiTaQYo0E

7. Three examples of compact companion candidates

This section concentrates on three candidates from the catalogue, examining their photometric modulations as obtained by other surveys, OGLE (Soszyński et al. 2016; Pawlak et al. 2016), ASAS-SN (Shappee et al. 2014; Kochanek et al. 2017), and ZTF (Bellm et al. 2019), and compares them with the modulation of *Gaia*. Then we discuss their candidacy of reliably having compact object companions. This exemplifies the potential of the candidates in the catalogue.

The three stars are marked in the pertinent figures above, except for *Gaia* DR3 4070409432055253760, which does not have an extinction estimate and therefore does not appear in Fig. 6. *Gaia* DR3 4042390512917208960 is the second brightest candidate in our catalogue. It is marked in bold in Table 3 and Fig. 9.

Figures 10–12 show the available photometry of the three examples, folded with the *Gaia* period. It clearly displays the *Gaia* modulation in the different independent data sets. Table 4 lists some parameters of the photometric analysis of the light curves of the three examples: source identifier, variability classification, second harmonic Fourier coefficient with its uncertainty, and the mMMR and its lower-percentile value.

The first star, *Gaia* DR3 4042390512917208960, was classified as an ellipsoidal variable by the OGLE team, but as a contact eclipsing binary (EW in their terminology) by the ASASSN-V group (Jayasinghe et al. 2020). Based on the *Gaia* and OGLE classification, we suggest that the system is an ellipsoidal variable. The relatively small amplitude of the ASAS-SN light curve is probably due to light contamination from a neighbouring star, as expected in the dense Galactic bulge. The second star, *Gaia* DR3 4070409432055253760, was classified as an ellipsoidal variable by the OGLE team, which reinforces our classification. The two stars have already been analysed by Gomel et al. (2021c) in a search for compact companions. The authors derived similar values for $\hat{q}_{\rm min}^{-1\sigma}$.

The third star, *Gaia* DR3 4056017172771375616, with the shortest period of the three systems, was classified as a contact binary (EC in their terminology) by the OGLE team. Although it is quite difficult to distinguish between the two types of modulations, the modulation shape is consistent with an ellipsoidal modulation, and follow-up observations are required to determine the correct variability.

Table 5 lists the astrophysical parameters of the three systems, including effective temperature, log gravity, metallicity, radius, mass, and stellar age, as derived by Fouesneau et al. (2023). The last column of the table lists the minimum mass of the secondary, derived from the mMMR of Table 3 and the primary mass. In parentheses we show the 15.9 percentile of the mass, using the $\hat{q}_{\rm min}^{-1\sigma}$ value. The second star does not have an estimate of the astrophysical parameters, and therefore no minimum secondary mass was derived.

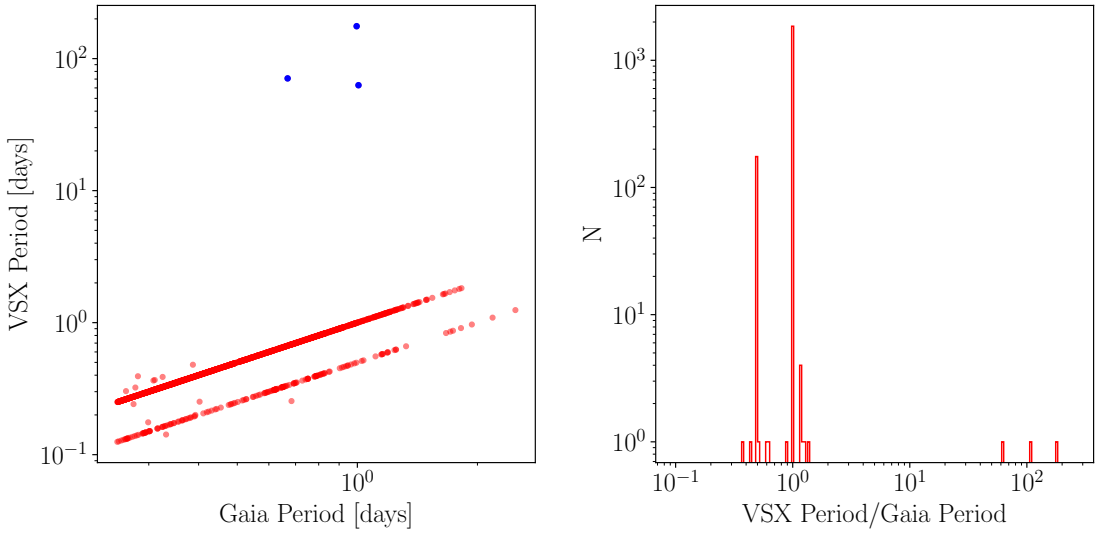

Fig. 7. Scatter plot (*left*) and histogram (*right*) of the 2044 VSX periods vs. those from *Gaia*.

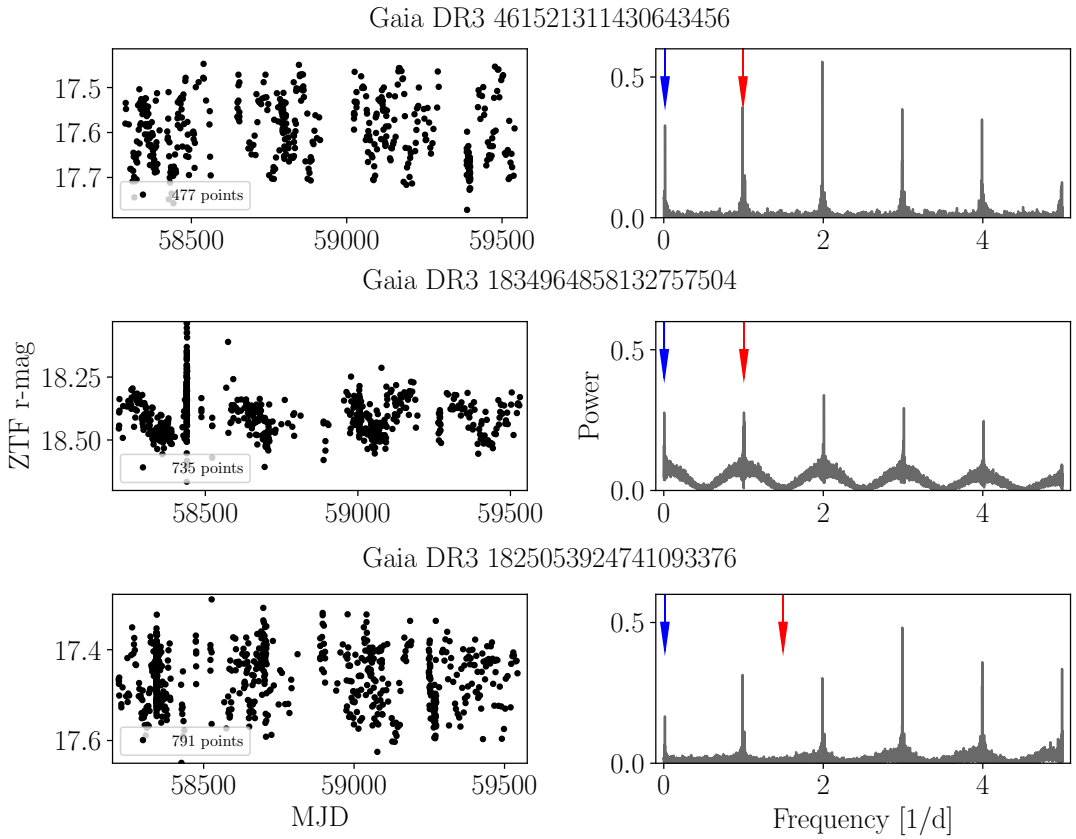

Fig. 8. Time series (*left*) and power spectra (*right*) of the ZTF project data for the three outlier sources. The red (blue) vertical line marks the frequency corresponding to the derived *Gaia* (ZFT) period.

The two stars with radius and mass in Table 5 display a radius that indicates a slightly evolved state. In principle, we tried to compose our catalogue of candidates with MS primaries alone to avoid Algol-type binaries, for which the evolved primary can outshine a more massive companion (see below). Nevertheless, the two examples of Table 5 are still good candidates, as their assumed secondaries, with a minimum mass of 3.2 and 1.9 $M_{\odot}$, are massive enough to be detected in the combined luminosity of the systems if they were MS components.

8. Discussion

We constructed a catalogue of 6306 variable stars that may have a massive, probably compact, companion on a short-period orbit according to the modulation of their ellipsoidal effect. As shown in Fig. 4, the period distribution of the candidates peaks at ~0.3–0.4 days, with a moderate decline towards longer periods. Our search is clearly more sensitive at short periods, and the decline is therefore probably due to selection effects. Out of the whole catalogue, we selected 262 candidates with an mMMR

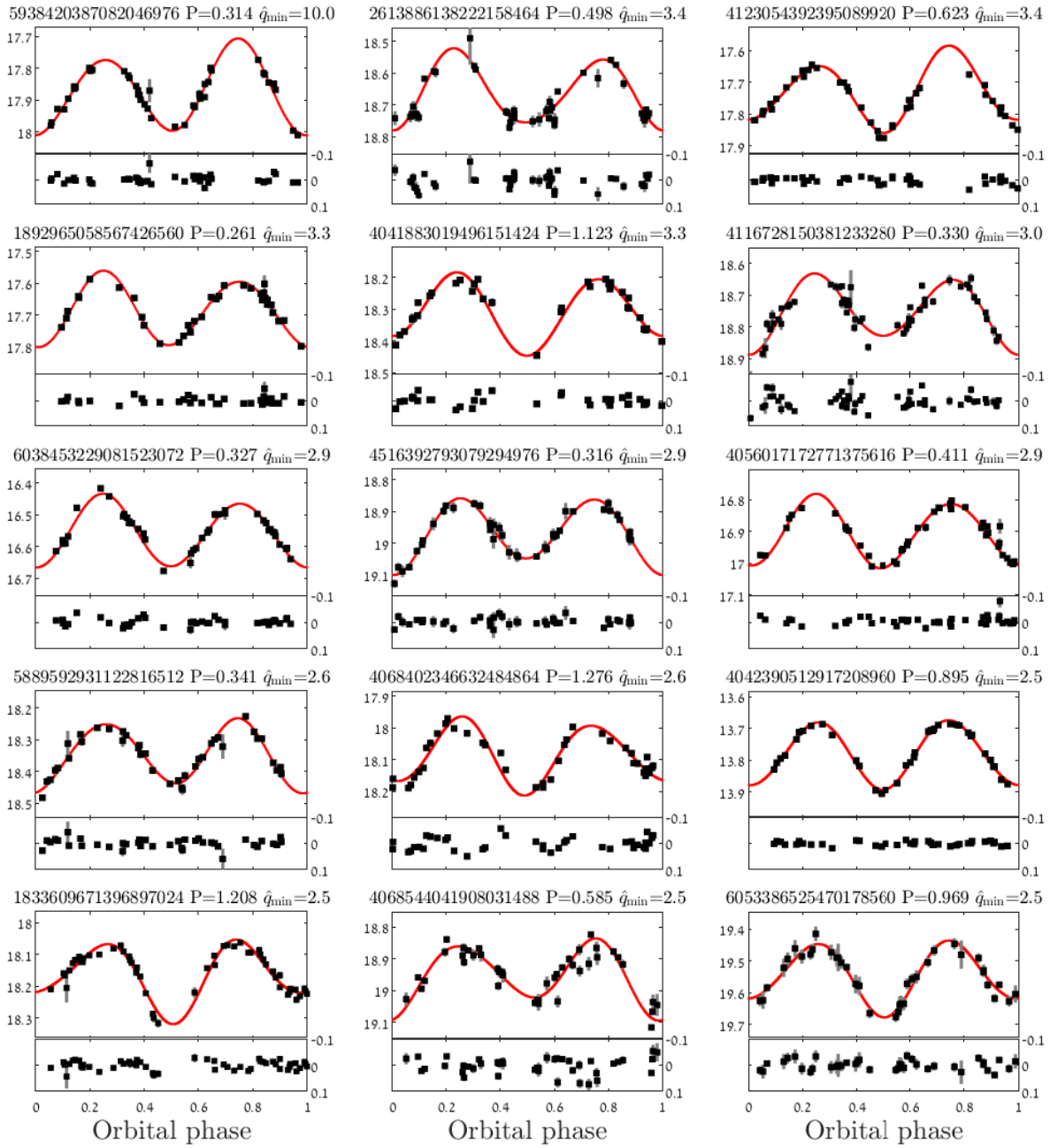

Fig. 9. Folded *Gaia* light curves in the *G* band of the first 15 candidates with $\hat{q}_{\rm min}^{-1\sigma} > 1$, in descending $\hat{q}_{\rm min}$ order. For each candidate, the *Gaia* DR3 id is given, together with the *Gaia* period in days and the value of $\hat{q}_{\rm min}$. The epoch of the second-harmonic minimum corresponds to phases 0 and 0.5, and a three-harmonics model is plotted with a solid red line. All curves are plotted with a mag range of 0.4 for convenience. The residuals are plotted in the *lower panels* and are shown between −0.1 and 0.1 mag for clarity. Marked identifiers are of *Gaia* DR3 4068402346632484864, which might be an RR Lyrae variable, discussed in Sect. 6, and *Gaia* DR3 4042390512917208960, which is one of our brightest candidates, discussed in Sect. 7.

higher than unity, with a higher probability to have a compact companion.

As mentioned above, the reality of the candidacy of the binaries in our catalogue and the sample of stars with a high mMMR in particular, depends on two main assumptions:

– The observed periodic variability is due to ellipsoidal modulation.
– The star is on the MS.

As shown, the two assumptions are not always fulfilled. Some systems are contact binaries (CB), with two components that are not detached. As pointed out above, it is not straightforward to distinguish between CBs and ellipsoidal variables. For example, *Gaia* DR3 4042390512917208960, discussed in Sect. 7, was classified by our pipeline and by OGLE as an ellipsoidal variable, but it is listed as a contact eclipsing binary by ASAS-SN. Nevertheless, we suggest that the contamination of the catalogue by contact binaries is not strong because CBs must by nature have short orbital periods, mostly shorter than 0.25 d, as shown by Rucinski (2010). We have avoided periodic variables with such short periods.

In other cases, the modulations might be due to single-star variability, such as stellar pulsation or rotation. One example is

Table 3. Fitted parameters of the first 15 candidates in descending $\hat{q}_{\rm min}$ order.

Gaia DR3	P $P_{\rm err}$ [day]	T_0 $T_{0,\rm err}$ [$BJD-2455197.5$]	$\overline{G}$ $\overline{G}_{\rm err}$ [mag]	$a_{1\rm c}$ $a_{1\rm c,err}$ [mag]	$a_{2\rm c}$ $a_{2\rm c,err}$ [mag]	$a_{3\rm c}$ $a_{3\rm c,err}$ [mag]	$a_{1\rm s}$ $a_{1\rm s,err}$ [mag]	$a_{2\rm s}$ $a_{2\rm s,err}$ [mag]	$a_{3\rm s}$ $a_{3\rm s,err}$ [mag]	N	$\hat{q}_{\rm min}$	$\hat{q}_{\rm min}^{-1\sigma}$
5938420387082046976	0.314117 0.000054	2244.03610 0.00056	17.8719 0.0018	0.0098 0.0028	0.1315 0.0036	−0.0026 0.0026	0.0226 0.0033	0.0000 0.0021	−0.0115 0.0035	43	10.0	5.6
2613886138222158464	0.49774 0.00012	2423.3476 0.0020	18.6571 0.0039	−0.0103 0.0047	0.1105 0.0065	0.0229 0.0067	−0.0110 0.0067	0.0000 0.0046	0.0079 0.0057	46	3.4	2.1
4123054392395089920	0.62299 0.00021	2425.4947 0.0013	17.7272 0.0031	−0.0101 0.0023	0.1104 0.0047	−0.0109 0.0029	0.0220 0.0055	0.0000 0.0024	−0.0105 0.0038	43	3.4	2.2
1892965058567426560	0.261008 0.000044	2191.02880 0.00049	17.6875 0.0022	0.0023 0.0033	0.1097 0.0035	0.0008 0.0028	−0.0062 0.0028	0.0000 0.0026	0.0113 0.0033	36	3.3	2.2
4041883019496151424	1.12284 0.00077	2355.7487 0.0054	18.3060 0.0036	−0.0314 0.0057	0.1097 0.0061	0.0003 0.0052	−0.0068 0.0055	0.0000 0.0063	0.0041 0.0054	34	3.3	2.1
4116728150381233280	0.330273 0.000043	2487.1291 0.0014	18.7504 0.0035	0.0175 0.0059	0.1078 0.0074	0.0123 0.0061	−0.0068 0.0061	0.0000 0.0040	0.0032 0.0059	53	3.0	1.9
6038453229081523072	0.327324 0.000082	2105.02175 0.00072	16.5562 0.0020	−0.0002 0.0035	0.1073 0.0042	0.0019 0.0037	−0.0101 0.0033	0.0000 0.0023	0.0057 0.0031	41	2.9	2.0
4516392793079294976	0.316059 0.000046	2159.86061 0.00074	18.9664 0.0019	0.0214 0.0032	0.1066 0.0035	0.0048 0.0029	0.0014 0.0028	0.0000 0.0026	0.0034 0.0033	41	2.9	1.9
4056017172771375616	0.410707 0.000093	2394.25673 0.00078	16.9046 0.0016	−0.0038 0.0023	0.1066 0.0031	−0.0008 0.0024	−0.0049 0.0027	0.0000 0.0024	0.0112 0.0028	44	2.9	1.9
5889592931122816512	0.341463 0.000081	2204.82654 0.00084	18.3464 0.0021	0.0162 0.0031	0.1044 0.0037	−0.0004 0.0030	−0.0033 0.0033	0.0000 0.0026	−0.0129 0.0034	39	2.6	1.8
4068402346632484864[(1)]	1.27615 0.00079	2356.9575 0.0056	18.0847 0.0044	−0.0103 0.0062	0.1043 0.0070	−0.0132 0.0062	−0.0015 0.0064	0.0000 0.0055	0.0135 0.0061	39	2.6	1.6
4042390512917208960[(2)]	0.89522 0.00046	2383.8996 0.0014	13.7822 0.0015	0.0000 0.0022	0.1039 0.0022	−0.0074 0.0023	0.0046 0.0020	0.0000 0.0020	0.0012 0.0019	38	2.5	1.8
1833609671396897024	1.20849 0.00074	2202.2576 0.0028	18.1657 0.0028	−0.0286 0.0054	0.1035 0.0048	−0.0215 0.0038	−0.0010 0.0030	0.0000 0.0031	−0.0083 0.0038	53	2.5	1.7
4068544041908031488	0.58456 0.00025	2430.2668 0.0026	18.9518 0.0043	0.0258 0.0063	0.1033 0.0064	0.0116 0.0064	−0.0027 0.0058	0.0000 0.0057	−0.0153 0.0058	43	2.5	1.6
6053386525470178560	0.96892 0.00052	2206.1084 0.0033	19.5447 0.0035	−0.0177 0.0045	0.1032 0.0055	−0.0122 0.0053	0.0016 0.0053	0.0000 0.0042	−0.0040 0.0047	40	2.5	1.6

Notes. [(1)]Might be an RR Lyrae variable, discussed in Sect. 6. [(2)]One of our brightest candidates, discussed in Sect. 7. The full table is available at the CDS.

probably *Gaia* DR3 4068402346632484864, whose folded light curve resembles an RR Lyrae ab-type modulation, as shown in Fig. 9. Furthermore, RR Lyrae c-type variables may mimic ellipsoidal variability better. However, we suggest that only a few single-star variables are hidden in the catalogue because the CU7 classifier is highly efficient (Rimoldini et al. 2023).

Finally, some of the stars in the catalogue might be real ellipsoidal variables but have an MS companion. In some cases, the derived mMMR is lower than unity. We nevertheless included them in the catalogue because the mMMR can be substantially lower than the actual minimum mass ratio, depending on the actual stellar mass and radius of the primary. In other cases, the primary star is slightly evolved and therefore might outshine an MS secondary. However, as shown in Fig. 6, a considerable portion of the catalogue stars with extinction estimates are on the main sequence, and even cases with slightly evolved stars, such as the two examples discussed in Sect. 7, cannot hide an MS companion.

Nevertheless, despite all cautious measures, many of the candidates of the catalogue may not have a compact object companion. Therefore, only spectroscopic radial-velocity (RV) follow-up observations can validate the high mass ratio of the candidates. However, even before RV resources are devoted to follow-up observations, more photometric measurements can be added to the light curve to better study the shape of the periodic modulation, in particular at different photometric bands. This is expected in future *Gaia* data releases[12], for which the number of FoV transits is going to double, including the $G_{\rm BP}$ and $G_{\rm RP}$ measurements, which were barely used here. The mass, radius, and temperature of the primary star might also be measured. These can be obtained either from the stellar position on the CMD and/or from its spectral energy distribution, when infrared observations and parallax are available. Any deviation from the mass-radius-temperature relations of MS stars might indicate that either the primary is not on the MS or that the secondary substantially contributes to the brightness of the system, making the star a less attractive candidate for having a compact companion.

Another indication for a compact companion may come from X-ray observations (e.g., Forman et al. 1978; Voges et al. 1999; Evans et al. 2010; Webb et al. 2020). An example is the discussion of *Gaia* DR3 5966509571940818048 in Sect. 5.3. Some dormant compact objects might have temporal X-ray emission (e.g., Remillard & McClintock 2006; Belloni 2010) and therefore have not yet been detected as X-ray sources. Therefore, any X-ray survey or pointed observations of the best candidates can be very useful.

[12] https://www.cosmos.esa.int/web/gaia/release

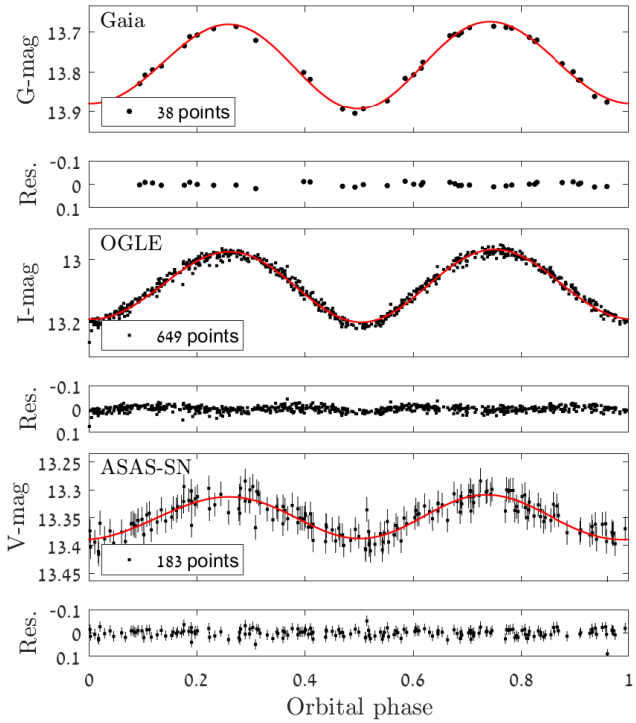

Fig. 10. Folded light curves of *Gaia* DR3 4042390512917208960 in the *Gaia G* (*top panel*), OGLE *I* (*middle panel*), and ASAS-SN *V* (*bottom panel*) bands. The orbital phase is calculated with a period of 0.89522 d and zero phase at BJD 2457581.3996, derived by the *Gaia* pipeline. A three-harmonics model is plotted with a solid line, and the residuals are plotted in the *lower panel*. The *G*- and *I*-band uncertainties, about 1 ppt, are too small to be shown.

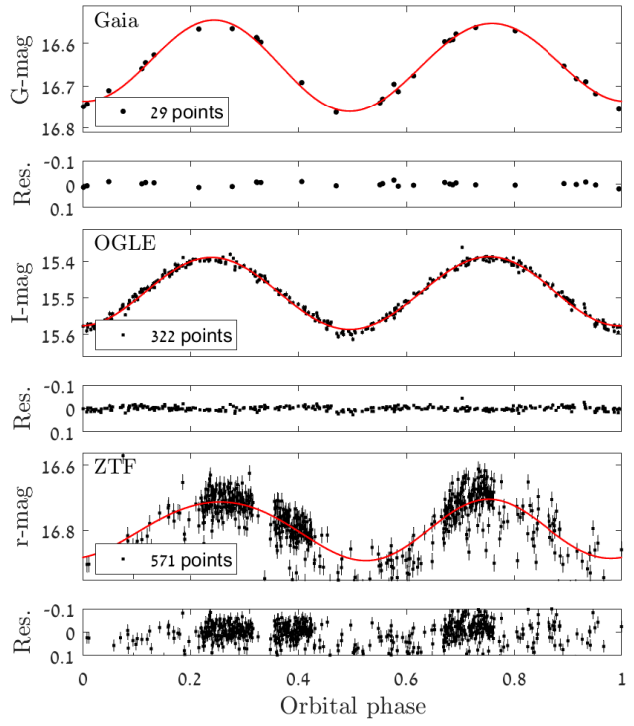

Fig. 11. Folded light curves of *Gaia* DR3 4070409432055253760 in the *Gaia G* (*top panel*), OGLE *I* (*middle panel*), and ZTF *r* (*bottom panel*) bands, as in Fig. 10. The orbital phase is calculated with a period of 0.64373 d and zero phase at BJD 2457449.2337, derived with the *Gaia* pipeline.

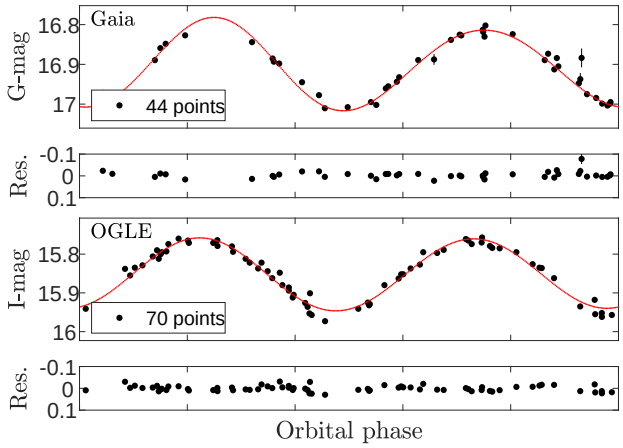

Fig. 12. Folded light curves of *Gaia* DR3 4056017172771375616 in the *Gaia G* (*top panel*) and OGLE *I* (*bottom panel*) bands, as in Fig. 10. The orbital phase is calculated with a period of 0.410707 d and zero phase at BJD 2457591.75673, derived with the *Gaia* pipeline.

Table 4. Parameters of the photometric analysis of light curves of the three candidates.

	Classification[(1)]	a_{2c} $a_{2c,err}$ [mag]	$\hat{q}_{min}$ $\hat{q}^{-1\sigma}_{min}$
DR3 4042390512917208960	ELL	0.1039	2.5
G band		0.0022	1.8
OGLE-BLG-ELL-012306	ELL	0.11219	2.5
I band		0.00053	1.7
ASASSN-V J175613.02-335233.3	EW	0.0386	
V band		0.0018	
DR3 4070409432055253760	ELL	0.0995	2.1
G band		0.0027	1.5
OGLE-BLG-ELL-013007	ELL	0.09659	1.4
I band		0.00058	1.0
ZTF 282116300002763		0.0885	
r band		0.0085	
DR3 4056017172771375616	ELL	0.1066	2.9
G band		0.0031	1.9
OGLE-BLG-ECL-106459	EC	0.0880	
I band		0.0024	

Notes. [(1)]Classification abbreviations represent ellipsoidal variable (ELL), eclipsing contact binary (EC), or a contact binary of EW type (EW).

When follow-up RV is performed, only a few measurements with medium precision, on the order of 10 km s^{-1}, should be enough to establish the binarity and the minimum mass ratio of each system because the presumed orbital period is known and the expected RV amplitude is on the order of 100 km s^{-1}. Unfortunately, *Gaia* RVS measurements (Katz et al. 2019) are not suitable for the candidates of our catalogue because their stellar brightness and/or temperature are not in the RVS effective range. Thus, our candidates necessitate a dedicated program of follow-up observations.

An RV follow-up project like this can be done, for example, with multi-object spectrographs such as SDSS-V (Kollmeier et al. 2017) and the upcoming 4MOST (de Jong et al. 2019). The magnitude limit of these spectrographs clearly depends on the exposure time, spectral information of the systems, and on the required RV precision. All in all, we assume that for our purpose, the limit is about 19th mag. This limit is

Table 5. Astrophysical parameters of the three candidates.

Gaia DR3	$T_{\rm eff}$ [K]	$\log g$	FeH [dex]	R [$R_\odot$]	M [$M_\odot$]	age [Gyr]	$M_{2,\rm min}$ [$M_\odot$]
4042390512917208960	5036^{+442}_{-231}	$4.18^{+0.13}_{-0.13}$	$-0.23^{+0.30}_{-0.77}$	$3.16^{+0.16}_{-0.13}$	$1.81^{+0.06}_{-0.05}$	$1.4^{+0.2}_{-0.2}$	4.6 (3.2)
4070409432055253760	4024^{+71}_{-67}	$4.80^{+0.05}_{-0.06}$	$0.10^{+0.05}_{-0.10}$				
4056017172771375616	4282^{+52}_{-70}	$4.70^{+0.07}_{-0.09}$	$-0.00^{+0.07}_{-0.10}$	$1.68^{+0.24}_{-0.16}$	$0.99^{+0.07}_{-0.05}$	$11.5^{+1.6}_{-2.2}$	2.8 (1.9)

marked in Figs. 1 and 2, indicating that most of our candidates can be followed by these spectrographs.

The catalogue presented here, although the level of contamination is unknown, has the capacity of opening a new window for studying short-period binaries with a compact object companion, either a BH or an NS, and sometimes a white dwarf, when some of the candidates are confirmed by additional observations.

Acknowledgements. We are indebted to the referee, who contributed illuminating comments and suggestions on the previous version of the manuscript, helping us improve substantially the paper. This research was supported by Grant No. 2016069 of the United States-Israel Binational Science Foundation (BSF) and by Grant No. I-1498-303.7/2019 of the German-Israeli Foundation for Scientific Research and Development (GIF) to TM. We have made use of data from the ESA space mission *Gaia*, processed by the *Gaia* Data Processing and Analysis Consortium (DPAC). Funding for some of the DPAC participants has been provided by *Gaia* Multilateral Agreement, which include, for Switzerland, the Swiss State Secretariat for Education, Research and Innovation through the ESA Prodex program, the "Mesures d'accompagnement", the "Activités Nationales Complémentaires", the Swiss National Science Foundation, and the Early Postdoc.Mobility fellowship; for Belgium, the BELgian federal Science Policy Office (BELSPO) through PRODEX grants; for Italy, Istituto Nazionale di Astrofisica (INAF) and the Agenzia Spaziale Italiana (ASI) through grants I/037/08/0, I/058/10/0, 2014-025-R.0, and 2014-025-R.1.2015 to INAF (PI M.G. Lattanzi); for France, the Centre National d'Etudes Spatiales (CNES). Part of this research has received funding from the European Research Council (ERC) under the European Union's Horizon 2020 research and innovation programme (Advanced Grant agreements N670519: MAMSIE "Mixing and Angular Momentum tranSport in MassIvE stars"). This research has made use of NASA's Astrophysics Data System, the VizieR catalogue access tool, CDS, Strasbourg, France.

References

Anders, F., Khalatyan, A., Chiappini, C., et al. 2019, A&A, 628, A94
Andrae, R., Fouesneau, M., Creevey, O., et al. 2018, A&A, 616, A8
Audard, M., Briggs, K. R., Grosso, N., et al. 2007, A&A, 468, 379
Bellm, E. C., Kulkarni, S. R., Graham, M. J., et al. 2019, PASP, 131, 018002
Belloni, T. M. 2010, States and Transitions in Black Hole Binaries, 794, 53
Bernabei, S., & Polcaro, V. F. 2001, A&A, 371, 123
Bodensteiner, J., Shenar, T., Mahy, L., et al. 2020, A&A, 641, A43
Breivik, K., Chatterjee, S., & Larson, S. L. 2017, ApJ, 850, L13
Budding, E., Erdem, A., Çiçek, C., et al. 2004, A&A, 417, 263
Chen, X., Zhang, X., Li, Y., et al. 2020, ApJ, 895, 136
Claret, A. 2019, Res. Notes Am. Astron. Soc., 3, 17
Clavel, M., Dubus, G., Casares, J., & Babusiaux, C. 2021, A&A, 645, A72
Contreras Ramos, R., Minniti, D., Gran, F., et al. 2018, ApJ, 863, 79
Corral-Santana, J. M., Casares, J., Muñoz-Darias, T., et al. 2016, A&A, 587, A61
de Jong, R. S., Agertz, O., Berbel, A. A., et al. 2019, The Messenger, 175, 3
de Marchi, F., Poretti, E., Montalto, M., Desidera, S., & Piotto, G. 2010, A&A, 509, A17
Drake, A. J., Graham, M. J., Djorgovski, S. G., et al. 2014, ApJS, 213, 9
Eggleton, P. P. 1983, ApJ, 268, 368
El-Badry, K., & Burdge, K. B. 2022, MNRAS, 511, 24
El-Badry, K., & Quataert, E. 2021, MNRAS, 502, 3436
El-Badry, K., Seeburger, R., Jayasinghe, T., et al. 2022, MNRAS, 512, 5620
Evans, I. N., Primini, F. A., Glotfelty, K. J., et al. 2010, ApJS, 189, 37
Eyer, L., Audard, M., Holl, B., et al. 2023, A&A, 674, A13 (*Gaia* DR3 SI)
Fabian, A. C., Rees, M. J., Stella, L., & White, N. E. 1989, MNRAS, 238, 729
Faigler, S., & Mazeh, T. 2011, MNRAS, 415, 3921
Faigler, S., Kull, I., Mazeh, T., et al. 2015, ApJ, 815, 26
Fedurco, M., & Parimucha, Š. 2018, Ap&SS, 363, 267
Forman, W., Jones, C., Cominsky, L., et al. 1978, ApJS, 38, 357
Fouesneau, M., Frémat, Y., Andrae, R., et al. 2023, A&A, 674, A28 (*Gaia* DR3 SI)
Fruth, T., Cabrera, J., Chini, R., et al. 2013, AJ, 146, 136
Gaia Collaboration (Brown, A. G. A., et al.) 2018, A&A, 616, A1
Gomel, R., Faigler, S., & Mazeh, T. 2021a, MNRAS, 504, 2115
Gomel, R., Faigler, S., & Mazeh, T. 2021b, MNRAS, 501, 2822
Gomel, R., Faigler, S., Mazeh, T., & Pawlak, M. 2021c, MNRAS, 504, 5907
Irrgang, A., Geier, S., Kreuzer, S., Pelisoli, I., & Heber, U. 2020, A&A, 633, L5
Jayasinghe, T., Stanek, K. Z., Kochanek, C. S., et al. 2020, MNRAS, 491, 13
Jayasinghe, T., Stanek, K. Z., Thompson, T. A., et al. 2021, MNRAS, 504, 2577
Jayasinghe, T., Thompson, T. A., Kochanek, C. S., et al. 2022, MNRAS, 516, 5945
Katz, D., Sartoretti, P., Cropper, M., et al. 2019, A&A, 622, A205
Kochanek, C. S., Shappee, B. J., Stanek, K. Z., et al. 2017, PASP, 129, 104502
Kollmeier, J. A., Zasowski, G., Rix, H. W., et al. 2017, ArXiv e-prints [arXiv:1711.03234]
Kopal, Z. 1959, Close Binary Systems (London: Chapman & Hall)
Kuhn, M. A., Medina, N., Getman, K. V., et al. 2017, AJ, 154, 87
Liu, J., Zhang, H., Howard, A. W., et al. 2019, Nature, 575, 618
Mashian, N., & Loeb, A. 2017, MNRAS, 470, 2611
Mazeh, T., & Faigler, S. 2020, MNRAS, 498, L58
Mennekens, N., & Vanbeveren, D. 2017, A&A, 599, A84
Metzger, M. R., & Schechter, P. L. 1998, AJ, 116, 469
Miller, V. R., Albrow, M. D., Afonso, C., & Henning, T. 2010, A&A, 519, A12
Morton, T. D. 2015, Astrophysics Source Code Library [record ascl:1503.010]
Muno, M. P., Baganoff, F. K., Bautz, M. W., et al. 2003, ApJ, 589, 225
Muno, M. P., Bauer, F. E., Bandyopadhyay, R. M., & Wang, Q. D. 2006, ApJS, 165, 173
Negu, S. H., & Tessema, S. B. 2018, Astron. Nachr., 339, 709
Nelson, C. A., & Eggleton, P. P. 2001, ApJ, 552, 664
Orosz, J. A., McClintock, J. E., Narayan, R., et al. 2007, Nature, 449, 872
Paczyński, B. 1971, ARA&A, 9, 183
Pawlak, M., Soszyński, I., Udalski, A., et al. 2016, Acta Astron., 66, 421
Rebull, L. M. 2001, AJ, 121, 1676
Remillard, R. A., & McClintock, J. E. 2006, ARA&A, 44, 49
Rimoldini, L., Eyer, L., Audard, M., et al. 2022, Gaia DR3 documentation Chapter 10: Variability, Gaia DR3 Documentation, 10
Rimoldini, L., Holl, B., Gavras, P., et al. 2023, A&A, 674, A14 (*Gaia* DR3 SI)
Rivinius, T., Baade, D., Hadrava, P., Heida, M., & Klement, R. 2020, A&A, 637, L3
Rowan, D. M., Stanek, K. Z., Jayasinghe, T., et al. 2021, MNRAS, 507, 104
Rucinski, S. 2010, in International Conference on Binaries: in Celebration of Ron Webbink's 65th Birthday, eds. V. Kalogera, & M. van der Sluys, AIP Conf. Ser., 1314, 29
Samadi Ghadim, A., Lampens, P., & Jassur, M. 2018, MNRAS, 474, 5549
Samus', N. N., Kazarovets, E. V., Durlevich, O. V., Kireeva, N. N., & Pastukhova, E. N. 2017, Astron. Rep., 61, 80
Shao, Y., & Li, X.-D. 2019, ApJ, 885, 151
Shappee, B., Prieto, J., Stanek, K. Z., et al. 2014, Am. Astron. Soc. Meet. Abstr., 223, 236
Shenar, T., Bodensteiner, J., Abdul-Masih, M., et al. 2020, A&A, 639, L6
Shikauchi, M., Kumamoto, J., Tanikawa, A., & Fujii, M. S. 2020, PASJ, 72, 45
Soszyński, I., Udalski, A., Szymański, M. K., et al. 2014, Acta Astron., 64, 177
Soszyński, I., Pawlak, M., Pietrukowicz, P., et al. 2016, Acta Astron., 66, 405
Thompson, T. A., Kochanek, C. S., Stanek, K. Z., et al. 2019, Science, 366, 637
van den Heuvel, E. P. J., & Tauris, T. M. 2020, Science, 368, eaba3282
Voges, W., Aschenbach, B., Boller, T., et al. 1999, A&A, 349, 389
Webb, N. A., Coriat, M., Traulsen, I., et al. 2020, A&A, 641, A136
Weldrake, D. T. F., & Bayliss, D. D. R. 2008, AJ, 135, 649
Wiktorowicz, G., Wyrzykowski, Ł., Chruslinska, M., et al. 2019, ApJ, 885, 1
Yamaguchi, M. S., Kawanaka, N., Bulik, T., & Piran, T. 2018, ApJ, 861, 21
Yi, T., Sun, M., & Gu, W.-M. 2019, ApJ, 886, 97
Zechmeister, M., & Kürster, M. 2009, A&A, 496, 577
Zheng, L.-L., Gu, W.-M., Yi, T., et al. 2019, AJ, 158, 179
Ziolkowski, J. 2014, MNRAS, 440, L61